Synthetic routes, characterization and photophysical properties of luminescent, surface functionalized nanodiamonds

Adam H. Day,[a] Samuel J. Adams,[a] Laia Gines,[b] Oliver A. Williams,[b] Benjamin R. G. Johnson,[c] Ian A. Fallis,[a] E. Joel Loveridge,[d] Gurmit S. Bahra,[e] Petra C. F. Oyston,[e] Juan Manuel Herrera,[f] and Simon J.A. Pope[a]*

[a]School of Chemistry, Main Building, Cardiff University, Cardiff, UK CF10 3AT; [b]School of Physics and Astronomy, Cardiff University, Cardiff, UK; [c] School of Physics and Astronomy, University of Leeds, UK; [d]Department of Chemistry, Swansea University, UK; [e] Defence Science and Technology Laboratory, Porton Down, Salisbury, Wiltshire, UK; [f] Departamento de Quımica Inorganica, Facultad de Ciencias, Universidad de Granada, Avda. Fuentenueva s/n, 18071, Granada, Spain.

Abstract

The functionalization of small diameter (*ca*. 50 nm) polycarboxylated nanodiamond particles using amide coupling methodologies in both water and acetonitrile solvent has been investigated. In this manner, the surfaces of nanodiamond particles were adorned with different luminescent moities, including a green fluorescent 1,8-naphthalimide moiety (**Nap-1**), and a red emitting ruthenium(II) tris-bipyridine complex (**Ru-1**), as well as dual functionalisation with both luminophores. Comprehensive characterization of the surface functionalized nanodiamonds has been achieved using a combination of dynamic light scattering, nanoparticle tracking analysis, transmission electron microscopy, X-ray photoelectron spectroscopy, zeta potential measurements, microwave plasma atomic emission spectroscopy and time-resolved photophysics. The tendency of the functionalized nanodiamonds to aggregate reflects the degree of surface substitution, yielding small aggregates with typical particle sizes *ca*. 150 nm. This is likely to be driven by the reduction of the zeta potential, concomitant with the conversion of surface charged carboxylate groups to neutral amide functions. The results show that luminescent nanodiamond materials can be synthesised with tuneable photophysical properties.[1]

[1] *Corresponding author Tel: (+44) 029-20879316 E-mail: popesj@cardiff.ac.uk

1. Introduction

Nanodiamond (ND) is the eponymous nanoscale material consisting of sp^3 hybridized carbon core with a graphitic (sp^2) or amorphous carbon shell, whose primary particle size is generally between 2–100 nm in diameter.[1] Generally termed in the literature as ultradispersed ND, detonation ND, or occasionally nanocrystalline diamond (usually specific to particles of less than 10 nm in diameter), ND is generally a black or dark grey powder in solid form due to the high degree of light scattering from the small crystal.[1] ND particles are produced through detonation of ordinance in a controlled atmosphere (generally producing particles up to 5 nm), [2,3] or through mechanical milling of high-pressure, high-temperature diamond synthesis from a carbon source.[4,5] Synthesis of an ND-Si wafer through chemical vapor deposition, which can be broken up through milling, yields particles with a relatively narrow size distribution. [6,7]

Interest in ND has developed rapidly over the last decade with a range of applications across the scientific disciplines, particularly the utility of its unique magnetic and optical properties.[8] Material applications are potentially vast, including in tribology and lubricants,[8] and as optical filters [9] and polymer composites.[10] Apparently low cytotoxicity,[11] coupled with multiple surface labelling routes lend ND toward biological applications,[12] such as bioimaging [12,13,14] and drug delivery.[15,16,17,18] The development of applications necessitates the ability to functionalize ND through chemical approaches. The surface of ND can be modified to introduce well known functional groups such as halides, amines,[19,20] alcohols,[21,22] and carboxylic acids, the latter two *via* oxidizing treatments.[23] These surface chemistries facilitate the covalent modification of ND.

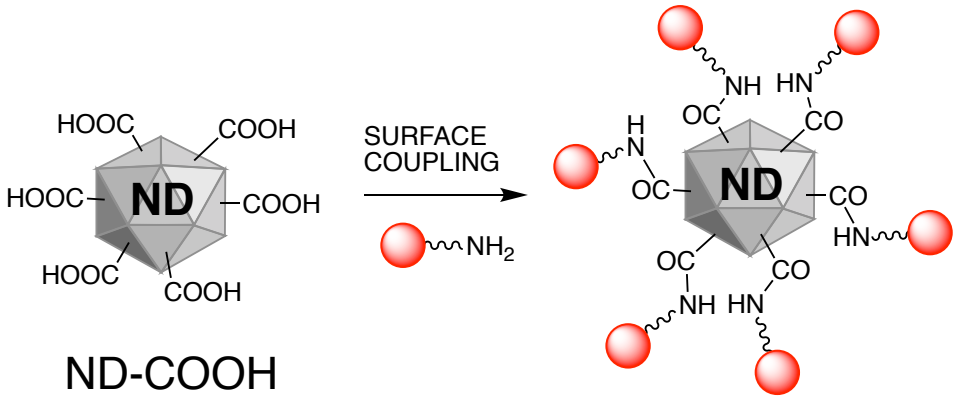

Figure 1. Cartoon representation of the surface functionalization of polycarboxylated nanodiamond (ND-COOH) using amide coupling.

Despite the simple accessibility apparent to a wide range of derivatives, polycarboxylated terminated ND (**ND-COOH**) has not been widely employed in the preparation of covalently functionalized ND materials (Figure 1). **ND-COOH** lends itself to facile surface modification, and examples of covalently modified **ND-COOH** include: the attachment of 5-adamantoyl-thymidine to ND (1-2 micron diameter particles) in bioassay development;[24] porphyrin functionalized ND towards optical power limiting materials;[25] a gadolinium(III) chelate functionalized ND as a prospective magnetic resonance imaging contrast agent;[26] and the attachment of a fluorescein dye to ND,[27] as well as DNA and protein conjugate examples.[28,29] Each of these examples provides different methodologies for the synthesis, employ differing purification procedures, and include varying degrees of characterization of the functionalized ND products. Thus, despite great potential, the direct amidation of the **ND-COOH** surface through the methods we describe (Figure 1) has only been employed in a limited number of examples, which did not extensively investigate the ND surface chemistry.

The aim of the current work was to utilise small diameter (*ca*. 50 nm) polycarboxylated **ND-COOH** and investigate different synthetic methodologies for its surface functionalization (Figure 1). Our focus was upon the addition of luminescent moieties to the surface of the ND, providing a useful spectroscopic handle for characterisation, but also yielding new ND materials with inherent and tuneable luminescent properties. We detail the extensive characterization of the functionalized ND particles suggesting an extremely broad scope for the future development of surface modified ND species using **ND-COOH**.

2. Experimental Section

2.1 General Experimental Considerations

All reagents and solvents were commercially available and were used without further purification if not stated otherwise. The nanodiamonds were sourced from MicroDiamant and Van Moppes.

For the measurement of ^{1}H and $^{13}C\{^{1}H\}$ NMR spectra, a Brüker Fourier 300 MHz, Brüker AVANCE III HD (400 MHz) or Brüker AVANCE (Cryo) III HD (500 MHz) was used. The obtained chemical shifts δ are reported in ppm and are referenced to the residual solvent signal. Spin-spin coupling constants *J* are given in Hz. Low-resolution mass spectra were obtained by the staff at Cardiff University. High-resolution mass spectra were carried out at the EPSRC National Mass Spectrometry Facility at Swansea University. High resolution mass spectral (HRMS) data were obtained on a Waters MALDI-TOF MicroMX at Cardiff University

or on a Thermo Scientific LTQ Orbitrap XL by the EPSRC UK National Mass Spectrometry Facility at Swansea University. IR spectra were obtained from a Shimadzu IR-Affinity-1S FTIR. Reference to spectroscopic data are given for known compounds. UV-Vis studies were performed on a Shimadzu UV-1800 spectrophotometer as water solutions (1×10^{-5} M). Photophysical data were obtained on a JobinYvon–Horiba Fluorolog spectrometer fitted with a JY TBX picosecond photodetection module as water solutions. Emission spectra were uncorrected and excitation spectra were instrument corrected. The pulsed source was a Nano-LED configured for 295 or 459 nm output operating at 1 MHz. Luminescence lifetime profiles were obtained using the JobinYvon–Horiba FluoroHub single photon counting module and the data fits yielded the lifetime values using the provided DAS6 deconvolution software. Quantum yield measurements were obtained on aerated water solutions of the complexes using $[Ru(bpy)_3](PF_6)_2$ in aerated MeCN as a standard ($\phi = 0.016$).[30]

Dynamic light scattering (DLS) and nanoparticle tracking analysis (NTA) measurements were performed to confirm the particles' size distribution. A Malvern Zetasizer Nano ZS equipped with a 633 nm laser in backscattering configuration (173 °) and a Malvern Nanosight LM10 equipped with a 635 nm laser were used respectively. Zeta potential measurements were made in the Malvern Zetasizer Nano ZS. Zeta potentials are reported at a given pH. Particle size distributions are the average of 100 × 30 s scans and zeta potential of 3 × 100 scans. The pH was measured by a Hanna Instruments HI 2211 pH meter. Nanoparticles were characterized by transmission electron microscopy (TEM) using a LIBRA 120 PLUS Carl Zeiss electron microscope operating at 120 kV. The probe sonicator used in these studies was a Sonics Vibra Cell VCX500. XPS measurements were performed using a Thermo Escalab 250 XPS with monochromated aluminium K-alpha X-ray source. The samples were dropcast onto gold and allowed to dry for analysis. The spot size was 500 μm with a power of 150 W. Detailed spectra of individual peaks were taken at energy of 20 eV with a step size of 0.1 eV, the number of scans for each element was optimised to give a good signal:noise for each element. Binding energy was calibrated by setting the carbon 1s peak to 285 eV. Detailed spectra had a Shirley or linear background fitted to them and peaks were fitted and deconvoluted using mixed Gaussian-Lorentzian fits (using CASAXPS). For MP-AES, samples were made as described in method 3 using 6 mL of starting nanodiamond suspension in acetonitrile before pelleting at the final centrifugation step. The mother liquor was decanted off and the particles dried in a vacuum desiccator overnight. The samples were then digested in 1 mL of aqua regia (CARE!), before diluting to 100 mL in UHQ water. The digested samples

were analysed on a XXXXXXXXXXXXX using 4 point calibrations with water blanks and emission intensities averaged over the ruthenium atomic emission wavelengths at 349.894, 372.693, 372.803 and 419.989 nm.

2.2 Surface functionalization of nanodiamond substrates and purification method

2.2.1 Synthesis Method 1

Nap-1 (aq.) was added to aqueous dispersions of **ND-COOH** (0.5 mg mL^{-1}) to give a final concentration of 2 mM in 3 ml. Solutions of N-hydroxysulfosuccinimide (10 mM) and 1-ethyl-3-(3-dimethylaminopropyl)carbodiimide (20 mM) were added, giving a final **ND-COOH** concentration of 0.25 mg mL^{-1}. Dispersions were buffered to pH 9.5 using CHES and stirred at 30°C for 16 hours. Samples were dialysed using a 3 K MWCO cellulose membrane at room temperature into water, sonicated for a total time of 10 minutes at 0°C and treated with another round of dialysis. A 1000-fold dilution was achieved over 12 h of equilibration at room temperature for each round of dialysis, resulting in the assumed dilution of any remaining substrate or coupling reagents or byproducts to 10^{-6} of their original concentration. Samples were then passed through a 0.22 μM PES membrane to remove any dust or large aggregates for analysis. Repeat measurements after 42 days were done with no further purification of filtration, samples were kept sealed in a dark, dry cupboard in the intervening time.

2.2.2 Synthesis Method 2

As for Method 1, but using a 50 mM borate buffer system (sodium tetraborate/boric acid) at pH 9.5.

2.2.3 Synthesis Method 3

ND-COOH was dispersed in acetonitrile (0.025 mg mL^{-1}) and then stirred at room temperature. A 2 mM solution of **Nap-1** or **Ru-1** was added together with 1-ethyl-3-(3-dimethylaminopropyl)carbodiimide (20 mg mL^{-1}), N-hydroxysuccinimide (20 mg mL^{-1}) and triethylamine (0.5 mL) for 24 hours. In the case of the mixed **Ru-1/Nap-1@ND**, the concentration of each was 1 mM. The functionalised nanodiamond was pelleted by centrifugation (4400 rpm, 30 minutes, Eppendorf micro-centrifuge), followed by subsequent washing steps in acetonitrile by probe sonication of the sample (30% amplitude, 30 minutes),

followed by centrifugation (4400 rpm, 30 minutes) until the supernatant was clear. The nanodiamond material was finally dispersed by probe sonication in water (1 mL, 30% amplitude, 30 minutes), followed by centrifugation (4400 rpm, 5 minutes) to remove residual titanium from the sonicator tip.

3. Results and Discussion

3.1 Syntheses of the luminescent groups

Two different types of luminescent species (Figure 2) were prepared for attachment to the ND surface: a green emitting 1,8-naphthalimide derivative (**Nap-1**), and a red emitting Ru(II) based luminophore (**Ru-1**). In both cases, the chromophores were functionalized with a flexible PEG-like group with an amine terminus to facilitate amide coupling to the nanodiamond surface. **Nap-1** was afforded in three steps from the commercially available 4-chloro-1,8-naphthalic anhydride, using conditions analogous to our previous reports[31] on related 1,8-naphthalimides.

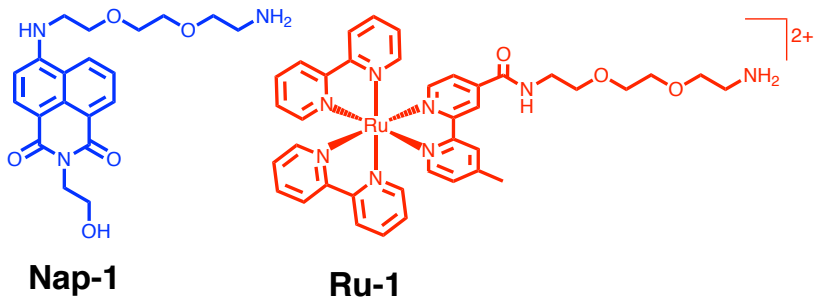

Figure 2. Structures of the amine terminated luminophores used to functionalize the surface of ND particles.

For **Ru-1**, a BOC-protected pro-ligand ($\mathbf{L}^{\mathbf{BOC}}$) was synthesized in two steps from 4-methyl-2,2´-bipyridine-4´-carboxylic acid. After reaction with $[Ru(bipy)_2Cl_2]$, the corresponding BOC-protected Ru(II) complex, $[Ru(bipy)_2(\mathbf{L}^{\mathbf{BOC}})][Cl]_2$, was isolated and then treated with trifluoroacetic acid in dichloromethane to yield the deprotected, amine-terminated cationic complex **Ru-1** as its dichloride salt. The synthesis procedures and characterization data for **Nap-1** and **Ru-1** are presented in the SI.

3.2 Synthesis and characterisation of surface-functionalized nanodiamond using a naphthalimide fluorophore

Nanodiamond suspensions were prepared from milled, acid treated nanodiamond particles obtained commercially. Prior to suspension, particles were treated at 420 Celcius over 2 hours in air to yield an oxidised surface.[23] Suspensions were prepared through repeated sonication and centrifugation in the desired solvent. We investigated the efficacy of three different

coupling protocols (Figure 3) using **Nap-1** and carboxylic acid terminated ND (**ND-COOH**) of approximately 50 nm diameter. In the first and second methods, **ND-COOH** was functionalized using an aqueous coupling method with 1-ethyl-3-(3-dimethylaminopropyl)carbodiimide (EDCI) and N-hydroxysulfosuccinimide (NHS) buffered to ca. pH 9.5 (using either N-cyclohexyl-2-aminoethanesulfonic acid or borate, respectively). Membrane dialysis was employed to remove free **Nap-1**, byproducts and buffer. The maintenance of elevated pH was critical to the efficient surface functionalization of ND with amine species. Our preliminary investigations showed that surface functionalization at pH 7 - 8 with **Nap-1** was achievable, but at a low degree of incorporation, as evidenced by the lack of color observed in particle suspensions following workup. In a third method, the coupling was investigated in polar organic media (MeCN) with EDCI and NHS coupling reagents, followed by purification by centrifugation. Full details of these protocols are described in the Experimental Section.

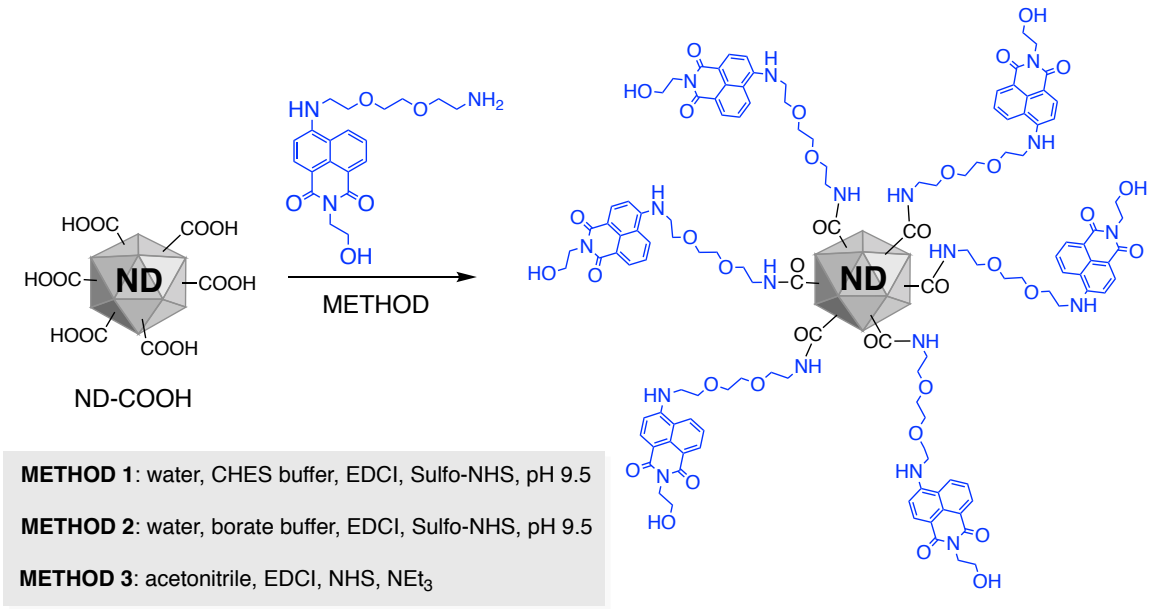

Figure 3. Cartoon representation of the synthetic routes to surface functionalized nanodiamond.

To characterize these new surface functionalized nanodiamond materials, a range of analytical and spectroscopic techniques was employed. For comparison, these structural and physical properties of **Nap-1@ND** arising from the three coupling protocols studied are shown in Table 1. Nanoparticle tracking analysis (NTA) measurements were utilized to obtain information on

the sizes of the functionalized nanodiamond particles, with sizes of *ca*. 150 nm for the **Nap-1@ND** systems compared with 53 nm for unfunctionalized **ND-COOH**. The particle diameters were also investigated by dynamic light scattering (DLS) measurements where **Nap-1@ND** was again found to be larger than **ND-COOH**, with sizes ranging from 143 to 228 nm. Interestingly, despite the apparent increase in particle size during the formation of the **Nap-1@ND** species, the polydispersity indices of the particles (determined by DLS) were broadly similar to **ND-COOH**. A visual comparison of the particle size distributions obtained from DLS and NTA data are presented in Figure 4.

Table 1. Structural information obtained from dynamic light scattering (DLS), nanoparticle tracking analysis (NTA) and zeta potential.

Sample	Particle diameter / nm		PDI	Zeta potential / mV
	DLS	NTA		
ND-COOH	62	53±1	0.13	–43.0[a]
Nap-1@ND (Method 1)	228	134±3	0.18	–12.8[b]
Nap-1@ND (Method 2)	143	146±5	0.39	–24.8[c]
Nap-1@ND (Method 3)	182	165±3	0.12	–19.5[d]

[a] Zeta potential recorded at pH 5.0; [b] pH 5.4; [c] pH 4.8; [d] pH 5.2.

Although the different polydispersity index (PDI) values obtained for **Nap-1@ND** may relate to the overestimation of larger particles in the DLS measurements giving a wider size distribution (Figure 1), the NTA analysis for **Nap-1@ND** from all three methods is broadly comparable. The DLS and NTA data therefore indicate that a small degree of aggregation of particles typically occurs during, or after, surface functionalization. The colloidal stability of the **Nap-1@ND** samples was investigated over a 7-day period using NTA analysis. Our results

showed that samples produced via Method 2 exhibited the best colloidal stability over that time period.

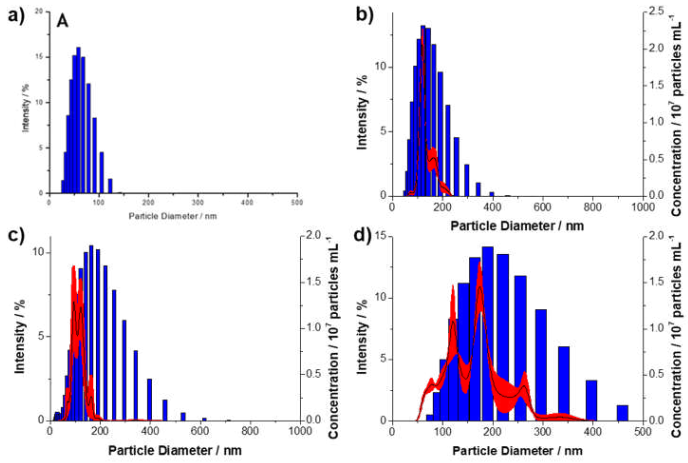

Figure 4. Superimposed DLS (blue bars) and NTA (blackline with red error) of (a) **ND-COOH**, (b) **Nap-1@ND** via Method 1, (c) **Nap-1@ND** via Method 2 and (d) **Nap-1@ND** via Method 3.

Zeta potentials (Table 1) for the surface functionalized nanodiamond were measured and provided further evidence of successful coupling. For reference, the zeta potential value for **ND-COOH** was recorded as –43.0 mV. In comparison, each of the **Nap-1@ND** samples gave recorded zeta potentials that were significantly less negative (ranging from –12.8 to –24.8 mV across the different coupling methods) and of lower magnitude. This change in zeta potential was attributed to the conversion of anionic carboxylate groups at the nanodiamond surface to charge neutral amide groups giving a net decrease in negative charge at the particle surface. A reduction in the magnitude of the zeta potential, and tendency of naphthalimide moities to stack, is likely to reduce colloidal stability in aqueous solution and therefore may help explain the observations from DLS and NTA analyses.

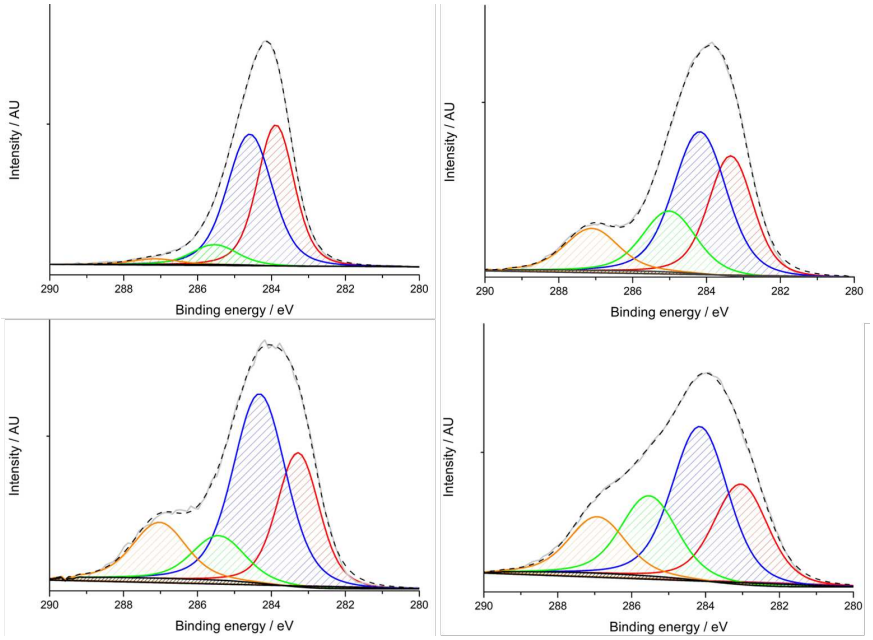

Figure 5. XPS data showing the deconvoluted C(1s) region of **ND-COOH** and **Nap-1@ND** obtained using preparatory Methods 1-3. C(1s-1) (red), C(1s-2) (blue), C(1s-3) (green) and C(1s-4) (orange) were fitted to the XPS spectral trace (light grey solid line) to give the fitted environment (black dashed line).

X-ray photoelectron spectroscopy (XPS) was undertaken to provide information on the surface groups of the ND samples. Firstly, analysis of unfunctionalized **ND-COOH** was obtained. Deconvolution of the C(1*s*) peak (Figure 5) of **ND-COOH** revealed two major and two minor components: C(1*s*-1) (B.E. = 283.9 eV), C (1*s*-2) (B.E. = 284.6 eV), C (1*s*-3) (B.E. = 285.5) and C (1*s*-4) (287.2), respectively. C (1s-1) corresponds to core sp^3 carbon, in good agreement with Shenderova *et al* (B.E. = 283.2 eV)[32] for smaller diameter ND; C(1*s*-2) corresponds to other surface located C-H and C-C content.[33] The minor components C(1*s*-3) and C(1*s*-4) correlate to oxidized surface carbon species C-O and C=O respectively, in good agreement with Lim *et al* for air oxidized ND of comparable size.[34] The C(1*s*) peak of **ND-COOH** is dominated by C(1*s*-1) and C(1*s*-2) (48 % and 43 % of total carbon composition), with the minor components, C(1*s*-3) (7%) and C(1*s*-4) (2%) representing very small proportions of carbon content in **ND-COOH**.

Although we have assumed that the majority of oxidised surface carbon in **ND-COOH** is present as carboxylate moieties, a range of other possible species are likely to be present. The components identified here may be made up of several sub-components, which are impossible to reliably elucidate through Gaussian fitting of the XPS data. Thus, the four carbon

components described above reasonably represent the ND surface environment of **ND-COOH**, which is predominantly made up of sp^3 hybridized carbon, surface located carbon species and oxygenated carbon species such as C=O and C-O.

Next, we considered the XPS analyses of the **Nap-1@ND** samples obtained by the three coupling methodologies and all revealed a consistent trend. Surface functionalization of **ND-COOH** (87.8 At% C, 0.4 At% N, 11.8 At% O) to give **Nap-1@ND** gave an increase in nitrogen (to ~10% At%) and oxygen (20.2% At%) content. These peaks were also observed in the C(1s) spectra of **Nap-1@ND**, but with an additional shoulder at 287.3-288.4 eV. This is consistent with an amide environment at the ND surface,[35] which we attribute to the presence of the covalently coupled naphthalimide moiety, at the ND surface.

Supporting transmission electron microscopy (TEM) images of the ND materials were also obtained (Figure 6). A comparison of the **ND-COOH** and **Nap-1@ND** samples revealed TEM images that are consistent with previous reports on similarly sized ND species.[36] The images for **ND-COOH** clearly show particles that are approximately in the 50 nm size range, consistent with the DLS and NTA data. Similarly, the TEM images of **Nap-1@ND** retain this appearance indicating that the morphology of the particles is not modified by surface functionalization with the **Nap-1** fluorophore. Again, the TEM images confirm that the sizes of the **Nap-1@ND** particles are consistent with the other characterization techniques, with no evidence of large agglomerations of particles.

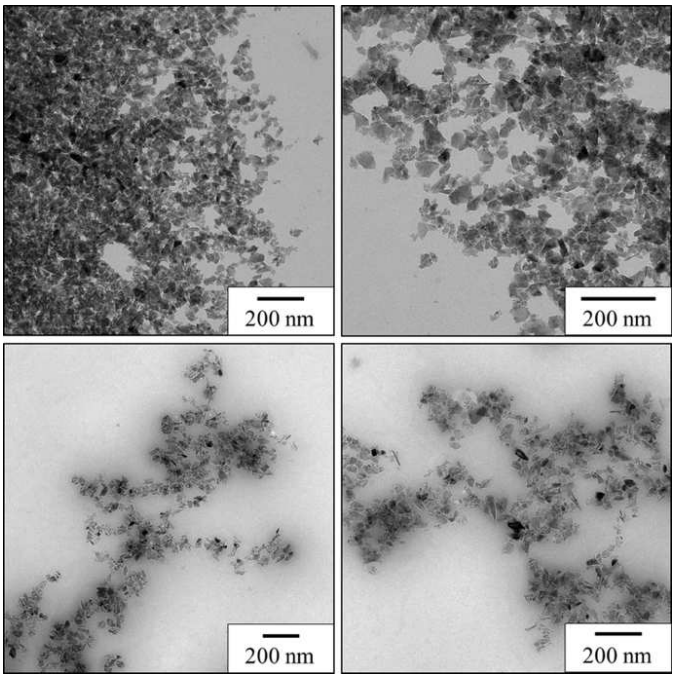

Figure 6. TEM images showing **ND-COOH** (top) and **Nap-1@ND** (bottom).

Having established the structural properties of the modified ND, the optical properties of the naphthalimide functionalized materials were determined using electronic absorption and luminescence spectroscopy. Figure 7 shows the absorption and emission spectra obtained from aqueous solutions of **Nap-1@ND**. Comparison of the UV-vis. absorption spectra of **Nap-1** and **Nap-1@ND** in aqueous solution clearly demonstrate the inclusion of the naphthalimide fluorophore. The characteristic naphthalimide based $\pi \rightarrow \pi^*$ and intramolecular charge transfer (ICT) bands[37] observed between 250-450 nm seen for **Nap-1** are clearly reproduced in the absorption spectrum of **Nap-1@ND**. Following irradiation of the ICT band at 440 nm, the luminescence spectrum of **Nap-1@ND** showed a broad peak centered at 540 nm (τ_{obs} = 4.1 ns). This compares with 543 nm (τ_{obs} = 3.9 ns) for free **Nap-1**, suggesting that the emissive properties of the 1,8-naphthalimide fluorophores are not only retained, but also relatively unperturbed, when covalently attached to the surface of ND.

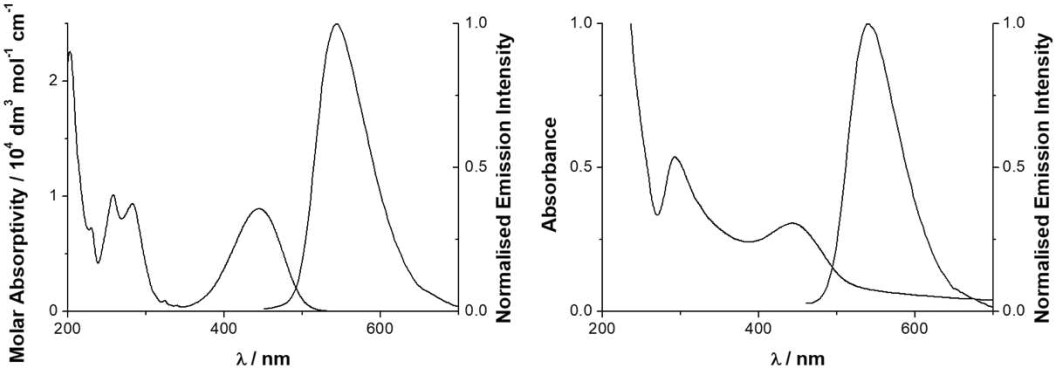

Figure 7. UV-vis. and luminescence spectra of showing **Nap-1** (left) and **Nap-1@ND** (right) in aqueous solution.

3.3 Co-functionalized ND: synthesis and characterisation of dual luminescent, hybrid materials

To further examine the applicability of the synthetic protocols for surface functionalization of ND, we expanded the repertoire by considering a cationic metal-based luminophore, **Ru-1** (Figure 2). Firstly, the synthesis of ND functionalized with **Ru-1** was undertaken (to give **Ru-1@ND)**, and secondly, we considered a co-functionalization approach with **Nap-1** thus giving a potentially hybrid material **Ru-1/Nap-1@ND**. The latter approach is particularly powerful when considering the tunability and multifunctional characteristics that could be imparted upon

a ND material. From a synthetic perspective, Method 3 (Figure 3) was utilised in all cases as this ensured solubility of the various reagents (Figure 8). In the case of **Ru-1/Nap-1@ND**, an equimolar solution of **Ru-1** and **Nap-1** was used in the surface coupling with **ND-COOH**. Details of the synthesis and purification procedures are given in the Experimental Section.

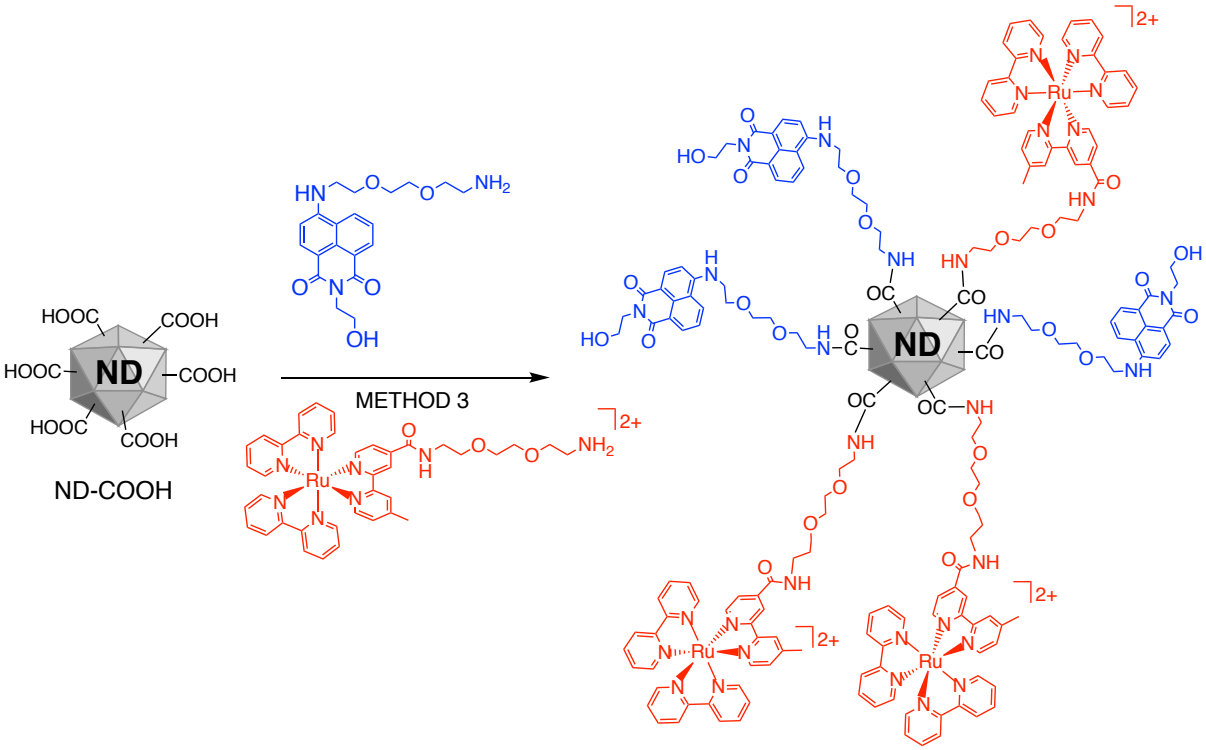

Figure 8. Cartoon representation of the synthetic route to co-functionalized ND decorated with naphthalimide (blue) and ruthenium (red) chromophores.

For **Ru-1@ND** and **Ru-1/Nap-1@ND**, the mean hydrodynamic diameters obtained by DLS were 182 nm (PDI = 0.14) and 151 nm (PDI = 0.23), respectively (Table 2). These values again represent an increase in particle size compared to **ND-COOH** and suggest modest aggregation of particles. The NTA data (Table 2) for all three samples correlates quite well (Figure 9) and supports the notion that the functionalized nanodiamond displays a small degree of aggregation.

Table 2. Structural information obtained from dynamic light scattering (DLS), nanoparticle tracking analysis (NTA) and zeta potential.

Sample	Particle Diameter / nm		PDI	Zeta Potential / mV
	DLS	NTA		
ND-COOH	62	53±1	0.13	–43.0[a]
Nap-1@ND (Method 3)	182	165±3	0.12	–19.5[b]
Ru-1@ND (Method 3)	171	171±8	0.14	+19.0[c]
Ru-1/Nap-1@ND (Method 3)	151	218±8	0.23	–4.5[d]

[a] Zeta potential recorded at pH 5.0; [b] pH 5.2; [c] pH 5.5; [d] pH 5.4.

The recorded zeta potentials (Table 2) of these nanodiamond samples (-19.5, -4.5 and +19.0 mV for **Nap-1@ND**, **Ru-1/Nap-1@ND** and **Ru-1@ND**, respectively), are all significantly less negative, and reduced in magnitude, when compared to **ND-COOH** particles. The variations in zeta potential are likely to be induced by the anticipated changes in surface charge when these different groups are added to the surface of the nanodiamond. We note that surface functionalization with dicationic **Ru-1** induces the most positive zeta potential in the series. Again, a reduction in the magnitude of the zeta potential is likely to reduce colloidal stability in solution, supporting the hypothesis of some aggregation.

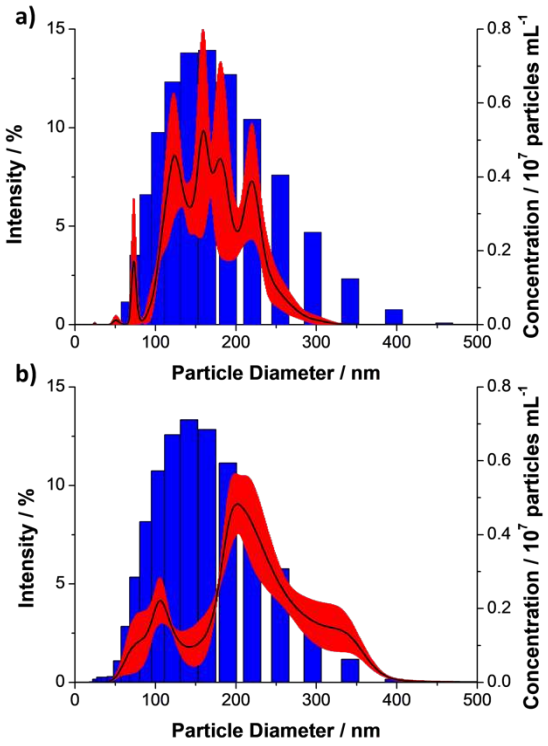

Figure 9. DLS (blue bar) and NTA (black line with red error bar) of (a) **Ru-1@ND** and (b) **Ru-1/Nap-1@ND**.

Analysis of the XPS spectra (Figure 10) for **Ru-1@ND** and **Ru-1/Nap-1@ND** again revealed the presence of the carbon (in particular amide), oxygen and nitrogen environments observed with the **Nap-1@ND** systems. Critically, for **Ru-1@ND** and **Ru-1/Nap-1@ND** the presence of the Ru($3d_{5/2}$) environment[38] at 279.2 eV (close to the C(1*s*) region of the XPS spectrum) was clearly observed. This was unequivocally confirmed following analysis by microwave plasma atomic emission spectroscopy (MP-AES) which demonstrated the presence of ruthenium in **Ru-1@ND** and **Ru-1/Nap-1@ND**. Ruthenium content was determined to be 1.4 and 1.1 wt% in **Ru-1@ND** and **Ru-1/Nap-1@ND**, respectively (see Table S1, Figures S1 and S2, Supporting Information).

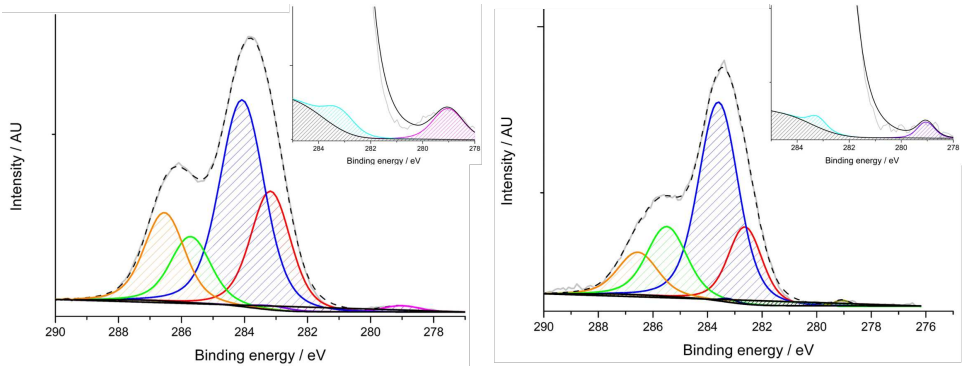

Figure 10. XPS spectra of the C(1s) region of **Ru-1@ND** (left) and **Ru-1/Nap-1@ND** (right) exhibiting carbon ascribed regions C(1s-1) (red), C(1s-2) (blue) C(1s-3) (green) and C(1s-4). Expansions show Ru($3d^{3/2}$) (magenta) and Ru($3d^{5/2}$) regions. Regions fitted to XPS trace (light grey line) to produce fitted trace (black dashed line).

TEM microscopy of the **Ru-1@ND** and **Ru-1/Nap-1@ND** materials (Figure 11) again revealed clusters of highly crystalline particles of *ca*. 50-150 nm size. This is consistent with the data obtained from DLS and NTA, again confirming the possibility of particle aggregation. The appearance of the particles in these images is clearly reminiscent of those obtained for **ND-COOH** and **Nap-1@ND** discussed earlier (Figure 6), and therefore confirms the integrity of the ND particle structure and morphology post-functionalization.

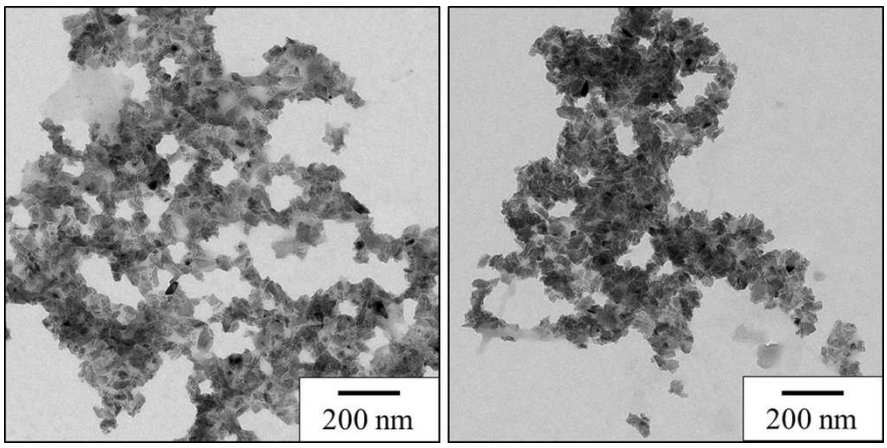

Figure 11. TEM images of **Ru-1@ND** (left) and co-functionalized **Ru-1/Nap-1@ND** (right).

Table 3. Photophysical data (in aerated water) obtained for the free luminophores and the corresponding functionalized ND species.

	UV-vis. absorption / nm	Luminescence / nm[a] (lifetime[b] / ns)
Nap-1	258, 283, 445	543 (4)
Nap-1@ND	288, 445	540 (5)
Ru-1	246, 287, 458	664 (287)
Ru-1@ND	281, 458	664 (332)
Ru-1/Nap-1@ND	283, 440*sh*	543 (5), 664 (328)

[a] using λ_{ex} = 405 or 450 nm; [b] using λ_{ex} = 295 nm.

The photophysical properties of the Ru(II) functionalized ND particles (Table 3) were determined in aqueous solution. The optical properties of **Nap-1** were discussed earlier, and for reference, **Ru-1** displayed visible absorption dominated by the expected metal-to-ligand charge transfer (^{1}MLCT) band in the visible region around 458 nm (in addition to ligand centered transitions < 300 nm). Once ND was functionalized with **Ru-1** to give **Ru-1@ND**, these absorption features were retained in the new material (Figure 8).

A comparison of the luminescence spectra in aerated aqueous solution showed (Figure 12) that the red emission of **Ru-1** (664 nm, lifetime of 287 ns), attributed to a ^{3}MLCT emitting state, was also present in the **Ru-1@ND** system, but with an extended lifetime of 332 ns (fitted to a single component exponential decay). The modest increase in ^{3}MLCT lifetime suggests that attachment to the ND surface does not quench the excited state, but rather, once it is covalently bound to the ND surface the difference in the chromophore locus subtly modulates the electronic properties of the Ru(II) luminophore.

In the case of the hybrid system, **Ru-1/Nap-1@ND**, the emission spectrum revealed a peak centered at 541 nm together with a shoulder at *ca*. 660 nm. The 541 nm peak is clearly reminiscent of the fluorescence spectra for **Nap-1** and **Nap-1@ND** and is thus ascribed to the ICT fluorescence band of the naphthalimide fluorophore. The additional long wavelength 660 nm feature is thus consistent with the presence of the ^{3}MLCT emissive state of **Ru-1** in this hybrid ND material. These assignments were further evidenced with measured lifetimes of 4.8 and 328 ns at emission wavelengths of 540 and 660 nm, respectively. These results correspond with the photophysical data obtained for both the **Ru-1@ND** and **Nap-1@ND** nanodiamond

systems. The lifetime data also suggests that the different chromophores are not within typical FRET (Förster resonance energy transfer) distances.

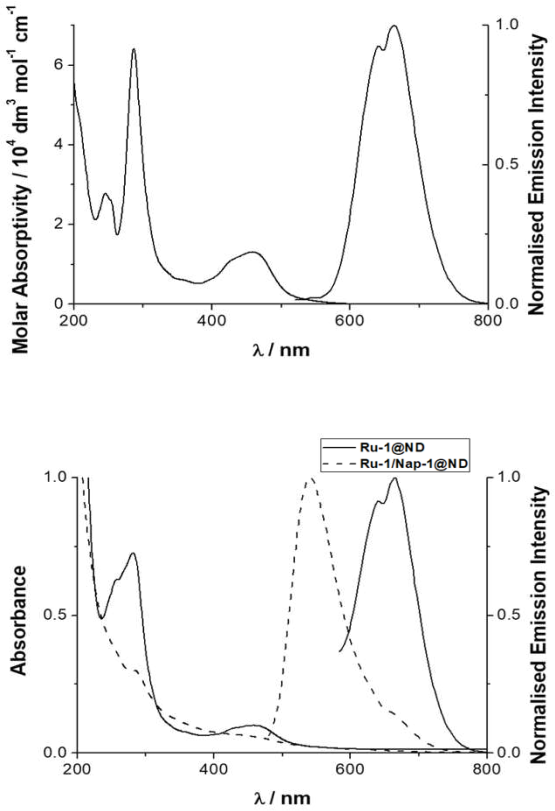

Figure 12. UV-vis. and luminescence spectra of showing **Ru-1** (top), **Ru-1@ND** and **Ru-1/Nap-1@ND** (bottom) in aqueous solution.

4. Conclusions

In summary, we have demonstrated that the surface of polycarboxylated ND can be functionalized with both organic and inorganic luminophores to produce hybrid materials with tuneable luminescent properties. The functionalized ND can be synthesised using typical peptide coupling methodologies, and purified either by membrane dialysis approaches or centrifugation. A combination of DLS, NTA, TEM and zeta potential measurements have clearly shown that the surface decoration of the ND leads to a small degree of aggregation: we observe that functionalized ND with very different zeta potentials (**Nap-1@ND** *vs*. **Ru-1@ND**) actually behave in a similar manner. Supporting MP-AES data confirmed the relative loadings of **Ru-1** in **Ru-1@ND** and **Ru-1/Nap-1@ND** samples. Steady state and time-resolved photophysical studies have been used to probe the surface-attached luminophores and describe

the luminescent nature of these new ND materials. The demonstrated ability to co-functionalize the ND surface with two different molecular entities opens the way to the design of bespoke ND materials with very broad applicability.

Acknowledgements

We thank the Ministry of Defence (UK) and The Leverhulme Trust (grant number RPG-2015-359) for funding. We also thank Cardiff University for support and the staff of the EPSRC Mass Spectrometry National Service (Swansea University).

Supporting Information

Includes synthetic details and characterization data for the **Nap-1** and **Ru-1** luminophores and their precursors, as well as supporting MP-AES data.

References

1) Schrand, A. M.; Hens, S.A.C.; Shenderova, O.A. "Nanodiamond Particles: Properties and Perspectives for Bioapplications" *Crit. Rev. Solid State Mater. Sci.* **2009**, *34*, 18-74
2) Greiner, N.R.; Phillips, D. S.; Johnson, J. D.; Volk, F. "Diamonds in detonation soot" *Nature* **1988**, *333*, 440-442
3) Danilenko, V.V. "On the history of the discovery of nanodiamond synthesis" *Phys. Solid State* **2004**, *46*, 595-599
4) Krueger, A.; Lang, D. "Functionality is Key: Recent Progress in the Surface Modification of Nanodiamond" *Adv. Funct. Mater.* **2012**, *22*, 890-906
5) Boudou, J.-P.; Curmi, P.A.; Jelezko, F.; Wrachtrup, J.; Aubert, P.; Sennour, M. *et al.* "High yield fabrication of fluorescent nanodiamonds" *Nanotechnology* **2009**, *20*, 235602
6) Williams, O.A. "*Nanodiamond*"; The Royal Society of Chemistry; **2014**; 253
7) Liu, Y.; Gu, Z.; Margrave, J.L.; Khabashesku, V.N. "Functionalization of Nanoscale Diamond Powder: Fluoro-, Alkyl-, Amino-, and Amino Acid-Nanodiamond Derivatives" *Chem. Mater.* **2004**, *16*, 3924-3930
8) Mochalin, V.N.; Shenderova, O.A.; Ho, D.; Gogotsi, Y. "The properties and applications of nanodiamonds" *Nature Nanotech.* **2012**, *7*, 11-23

9) Vanyukov, V.V.; Mikheev, G.M.; Mogileva, T.N.; Puzyr, A.P.; Bondar, V.S.; Svirko, Y.P. "Near-IR nonlinear optical filter for optical communication window" *Appl. Opt., AO* **2015**, *54*, 3290-3293

10) Behler, K.D.; Stravato, A.; Mochalin, V.; Korneva, G.; Yushin, G.; Gogtsi, Y. "Nanodiamond-Polymer Composite Fibers and Coatings" *ACS Nano* **2009**, *3*, 363-369

11) Schrand, A.M.; Huang, H.; Carlson, C.; Schlager, J.J.; Osawa, E.; Hussain, S.M. *et al*. "Are Diamond Nanoparticles Cytotoxic?" *J. Phys. Chem. B* **2007**, *111*, 2-7

12) Hens, S.C.; Cunningham, G.; Tyler, T.; Moseenkov, S.; Kuznetsov, V.; Shenderova, O. "Nanodiamond bioconjugate probes and their collection by electrophoresis" *Diam. Relat. Mater*. **2008**, *17*, 1858-1866

13) Edgington, R.; Spillane, K.M.; Papageorgiou, G.; Wray, W.; Ishiwata, H.; Labarca, M. *et al*. "Functionalisation of Detonation Nanodiamond for Monodispersed, Soluble DNA-Nanodiamond Conjugates Using Mixed Silane Bead-Assisted Sonication Disintegration" *Scientific Reports* **2018**, *8*, 728

14) Prabhakar, N.; Khan, M.H.; Peuria, M.; Chang, H-C.; Hanninen, P.E.; Rosenholm, J.M. "Intracellular Trafficking of Fluorescent Nanodiamonds and Regulation of Their Cellular Toxicity" *ACS Omega* **2017**, *2*, 2689-2693

15) Huang, H.; Pierstorff, E.; Osawa, E.; Ho, D. "Protein-Mediated Assembly of Nanodiamond Hydrogels into a Biocompatible and Biofunctional Multilayer Nanofilm" *ACS Nano* **2008**, *2*, 203-212

16) Huang, T. S.; Tzeng, Y.; Liu, Y.K.; Chen, Y.C.; Walker, K.R.; Guntupalli, R. *et al*. "Immobilization of antibodies and bacterial binding on nanodiamond and carbon nanotubes for biosensor applications" *Diam. Relat. Mater*. **2004**, *13*, 1098-1102

17) Nguyen, T.-T.-B.; Chang, H.-C.; Wu, V.W.-K. "Adsorption and hydrolytic activity of lysozyme on diamond nanocrystallites" *Diam. Relat. Mater*. **2007**, *16*, 872-876

18) Chow, E. K.; Zhang, X.Q.; Chen, M.; Lam, R.; Robinson, E.; Huang, H. *et al*. "Nanodiamond Therapeutic Delivery Agents Mediate Enhanced Chemoresistant Tumor Treatment" *Sci. Transl. Med*. **2011**, *3*, 73ra21

19) Koch, H.; Kulisch, W.; Popov, C.; Merz, R.; Merz, B.; Reithmaier, J.P. "Plasma amination of ultrananocrystalline diamond/amorphous carbon composite films for the attachment of biomolecules" *Diam. Relat. Mater*. **2011**, *20*, 254-258

20) Kulisch, W.; Popov, C.; Bliznakov, S.; Ceccone, G.; Gilliland, D.; Rauscher, H.; Sirghi, L.; Rossi, F. "Surface and bioproperties of nanocrystalline diamond/amorphous carbon nanocomposite films" *Thin Solid Films* **2007**, *515*, 8407-8411

21) Kruger, A.; Kataoka, F.; Ozawa, M.; Fujino, T.; Suzuki, Y.; Aleksenskii, A.E. *et al*. "Unusually tight aggregation in detonation nanodiamond: Identification and disintegration" *Carbon* **2005**, *43*, 1722-1730

22) Zheng, W.-W.; Hsieh, Y-H.; Chiu, Y-C.; Cai, S-J.; Cheng, C-L.; Chen, C. "Organic functionalization of ultradispersed nanodiamond: synthesis and applications" *J. Mater. Chem.* **2009**, *19*, 8432-8441

23) Osswald, S.;Yushin, G.; Mochalin, V.; Kucheyev, S.O.; Gogotsi, Y. "Control of sp^2/sp^3 Carbon Ratio and Surface Chemistry of Nanodiamond Powders by Selective Oxidation in Air" *J. Am. Chem. Soc.* **2006**, *128*, 11635-11642

24) Ushizawa, K.; Sato, Y.; Mitsumori, T.; Machinami, T.; Ueda, T.; Ando, T. "Covalent immobilization of DNA on diamond and its verification by diffuse reflectance infrared spectroscopy" *Chem. Phys. Lett.* **2002**, *351*, 105-108

25) Muller, O.; Pichot, V.; Merlat, L.; Schmidlin, L.; Spitzer, D. "Nonlinear optical behavior of porphyrin functionalized nanodiamonds: an efficient material for optical power limiting" *Appl. Optics* **2016**, *55*, 3801-3808

26) Sushkov, A. O.; Chisolm, N.; Lovchinsky, I.; Kubo, M.; Lo, P.K.; Bennett, S.D. *et al*. "All-Optical Sensing of a Single-Molecule Electron Spin" *Nano Lett.* **2014**, *14*, 6443-6448

27) Chang, I.P; Hwang, K.C.; Chiang, C-S. "Preparation of Fluorescent Magnetic Nanodiamonds and Cellular Imaging" *J. Am. Chem. Soc.* **2008**, *130*, 15476-15481

28) Christiaens, P; Vermeeren, V.; Wenmackers, S.; Daenen, M.; Haenen, K.; Nesladek, M. *et al*. "EDC-mediated DNA attachment to nanocrystalline CVD diamond films" *Biosens. Bioelectron.* **2006**, *22*, 170–177

29) Liu, Y; Sun, K.W. "Protein Functionalized Nanodiamond Arrays" *Nanoscale Res. Lett.* **2010**, *5*, 1045–1050

30) Frank, M.; Nieger, M.; Vogtle, F.; Belser, P.; von Zelewsky, A.; de Cola, L. *et al*. "Dinuclear Ru^{II} and/or Os^{II} complexes of bis-bipyridine bridging ligands containing adamantane spacers: synthesis, luminescence properties, intercomponent energy and electron transfer processes" *Inorg. Chim. Acta* **1996**, *242*, 281-291

31) For example: Langdon-Jones, E.E.; Williams, C.F.; Hayes, A.J.; Lloyd, D.; Coles, S.J.; Horton, P.N. *et al*. "Luminescent 1,8-Naphthalimide-Derived ReI Complexes: Syntheses, Spectroscopy, X-ray Structure and Preliminary Bioimaging in Fission Yeast Cells" *Eur. J. Inorg. Chem.* **2017**, 5279-5287

32) Shenderova, O.; Koscheev, A.; Zaripov, N.; Petrov, I.; Skryabin, Y.; Detkov, P. *et al*. "Surface Chemistry and Properties of Ozone-Purified Detonation Nanodiamonds" *J. Phys. Chem. C* **2011**, *115*, 9827-9837

33) Hamwi, A.; Latouche, C.; Marchand, V.; Dupuis, J.; Benoit, R. "Perfluorofullerenes: Characterization and structural aspects" *J. Phys. Chem. Solid* **1996**, *57*, 991-998

34) Lim, D.G.; Kim, K.H.; Kang, E.; Lim, S-H.; Ricci, J.; Sung, S.K. *et al*. "Comprehensive evaluation of carboxylated nanodiamond as a topical drug delivery system" *Int. J. Nanomedicine* **2016**, *11*, 2381-2395

35) Ruck-Braun, K.; Petersen, M.A.; Michalik, F.; Hebert, A.; Przyrembel, D.; Weber, C. *et al*. "Formation of Carboxy- and Amide-Terminated Alkyl Monolayers on Silicon(111) Investigated by ATR-FTIR, XPS, and X-ray Scattering: Construction of Photoswitchable Surfaces" *Langmuir* **2013**, *29*, 11758-11769

36) Gines, L.; Mandal, S.; Aschek-I-Ahmed; Cheng, C-L.; Sow, M.; Williams, O.A. "Positive zeta potential of nanodiamonds" *Nanoscale* **2017**, *9*, 12549-12555

37) Langdon-Jones, E.E.; Lloyd, D.; Hayes, A.J.; Wainwright, S.D.; Mottram, H.J.; Coles, S.J. *et al*. "Alkynyl-naphthalimide Fluorophores: Gold Coordination Chemistry and Cellular Imaging Applications" *Inorg. Chem.* **2015**, *54*, 6606-6615

38) Elmasides, C.; Kondarides, D.I.; Grunert, W.; Verykios, X.E. "XPS and FTIR Study of Ru/Al_2O_3 and Ru/TiO_2 Catalysts: Reduction Characteristics and Interaction with a Methane–Oxygen Mixture" *J. Phys. Chem. B* **1999**, *103*, 5227-5239

---

[1] Schrand, A. M.; Hens, S.A.C.; Shenderova, O.A. *Crit. Rev. Solid State Mater. Sci.* **2009**, *34*, 18

[2] Greiner, N.R.; Phillips, D. S.; Johnson, J. D.; Volk, F. *Nature* **1988**, *333*, 440

[3] Danilenko, V.V. *Phys. Solid State* **2004**, *46*, 595

[4] Krueger, A.; Lang, D. *Adv. Funct. Mater.* **2012**, *22*, 890

[5] Boudou, J.-P.; Curmi, P.A.; Jelezko, F.; Wrachtrup, J.; Aubert, P.; Sennour, M.; Balasubramanian, G.; Reuter, R.; Thorel, A.; Gaffet, E. *Nanotechnology* **2009**, *20*, 235602.

[6] Williams, O.A. *Nanodiamond*; The Royal Society of Chemistry; **2014**; 253

[7] Liu, Y.; Gu, Z.; Margrave, J.L.; Khabashesku, V.N. *Chem. Mater.* **2004**, *16*, 3924

[8] Mochalin, V.N.; Shenderova, O.A.; Ho, D.; Gogotsi, Y. *Nature Nanotechnology* **2012**, *7*, 11

[9] Vanyukov, V.V.; Mikheev, G.M.; Mogileva, T.N.; Puzyr, A.P.; Bondar, V.S.; Svirko, Y.P. *Appl. Opt., AO* **2015**, *54*, 3290
[10] Behler, K.D.; Stravato, A.; Mochalin, V.; Korneva, G.; Yushin, G.; Gogtsi, *ACS Nano* **2009**, *3*, 363
[11] Schrand, A.M.; Huang, H.; Carlson, C.; Schlager, J.J.; Osawa, E.; Hussain, S.M.; Dai, L. *J. Phys. Chem. B* **2007**, *111*, 2
[12] Hens, S.C.; Cunningham, G.; Tyler, T.; Moseenkov, S.; Kuznetsov, V.; Shenderova, O. *Diamond and Related Materials* **2008**, *17*, 1858;
[13] Edgington, R.; Spillane, K.M.; Papageorgiou, G.; Wray, W.; Ishiwata, H.; Labarca, M.; Leal-Ortiz, S.; Reid, G.; Webb, M.; Foord, J.; Meloshi, N.; Schaefer, A.T. *Scientific Reports* **2018**, *8*, 728.
[14] Prabhakar, N.; Khan, M.H.; Peuria, M.; Chang, H-C.; Hanninen, P.E.; Rosenholm, J.M. *ACS Omega* **2017**, *2*, 2689
[15] Huang, H.; Pierstorff, E.; Osawa, E.; Ho, D. *ACS Nano* **2008**, *2*, 203
[16] Huang, T. S.; Tzeng, Y.; Liu, Y.K.; Chen, Y.C.; Walker, K.R.; Guntupalli, R.; Liu, C. *Diamond and Related Materials* **2004**, *13*, 1098
[17] Nguyen, T.-T.-B.; Chang, H.-C.; Wu, V.W.-K. *Diam. Relat. Mater.* **2007**, *16*, 872.

[17] Chow, E. K.; Zhang, X.Q.; Chen, M.; Lam, R.; Robinson, E.; Huang, H.; Schaffer, D.; Osawa, E.; Goga, A.; Ho, D. *Sci. Transl. Med.* **2011**, *3*, 73ra21
[19] Koch, H.; Kulisch, W.; Popov, C.; Merz, R.; Merz, B.; Reithmaier, J.P. *Diam. Relat. Mater.* **2011**, *20*, 254;
[20] Kulisch, W.; Popov, C.; Bliznakov, S.; Ceccone, G.; Gilliland, D.; Rauscher, H.; Sirghi, L.; Rossi, F. *Thin Solid Films* **2007**, *515*, 8407
[21] Kruger, A.; Kataoka, F.; Ozawa, M.; Fujino, T.; Suzuki, Y.; Aleksenskii, A.E.; Vul, A.Y.; Osawa, E. *Carbon* **2005**, *43*, 1722;
[22] Zheng, W.-W.; Hsieh, Y-H.; Chiu, Y-C.; Cai, S-J.; Cheng, C-L.; Chen, C. *J. Mater. Chem.* **2009**, *19*, 8432
[23] Osswald, S.;Yushin, G.; Mochalin, V.; Kucheyev, S.O.; Gogotsi, Y. *J. Am. Chem. Soc.* **2006**, *128*, 11635
[24] Ushizawa, K.; Sato, Y.; takeshi, M.; Machinami, T.; Ueda, T.; Ando, T. *Chem. Phys. Lett.* **2002**, *351*, 105
[25] Muller, O.; Pichot, V.; Merlat, L.; Schmidlin, L.; Spitzer, D. *Appl. Optics* **2016**, *55*, 3801
[26] Sushkov, A. O.; Chisolm, N.; Lovchinsky, I.; Kubo, M.; Lo, P.K.; Bennett, S.D.; Akimov, A.; Walsworth, R.L.; Park, H.; Lukin, M.D. *Nano Lett.* **2014**, *14*, 6443
[27] Fluorescein I.P. Chang, K. C. Hwang, C-S. Chiang, *J. Am. Chem. Soc.* **2008**, *130*, 15476
[28] Christiaens, P; Vermeeren, V.; Wenmackers, S.; Daenen, M.; Haenen, K.; Nesladek, M.; van de Ven M.; Ameloot, M.; Michiels, L.; Wagner, P. EDC-mediated DNA attachment to nanocrystalline CVD diamond films. *Biosens. Bioelectron.* **2006**, 22, 170–177

[29] Liu, Y; Sun, K.W. Protein Functionalized Nanodiamond Arrays. *Nanoscale Res Lett* **2010** ***5***, 1045–1050
[30] Frank, M.; Nieger, M.; Vogtle, F.; Belser, P.; von Zelewsky, A.; de Cola, L.; Balzani, V.; Barigelletti, F.; Flamigni, L. *Inorg. Chim. Acta* **1996**, *242*, 281
[31] For example: Langdon-Jones, E.E.; Williams, C.F.; Hayes, A.J.; Lloyd, D.; Coles, S.J.; Horton, P.N.; Groves, L.M.; Pope, S.J.A. *Eur. J. Inorg. Chem.* **2017**, 5279
[32] Shenderova, O.; Koscheev, A.; Zaripov, N.; Petrov, I.; Skryabin, Y.; Detkov, P.; Turner, S.; Van Tedeloo, G. *J. Phys. Chem. C* **2011**, *115*, 9827
[33] Hamwi, A.; Latouche, C.; Marchand, V.; Dupuis, J.; Benoit, R. *J. Phys. Chem. Solid* **1996**, *57*, 991

[34] Lim, D.G.; Kim, K.H.; Kang, E.; Lim, S-H.; Ricci, J.; Sung, S.K.; Kwon, M.T.; Jeong, S.H. *Int. J. Nanomedicine* **2016**, *11*, 2381.
[35] Braun, K.; Peterson, M.A.; Michilak, F.; Hebert, A.; Przyrembel, D.; Weber, C.; Ahmed, S.A.; Kowarik, S.; Weinelt, M. *Langmuir* **2013**, *29*, 11758.
[36] Gines, L.; Mandal, S.; Aschek-I-Ahmed, Cheng, C-L.; Sow, M.; Williams, O.A. *Nanoscale* **2017**, *9*, 12549
[37] Langdon-Jones, E.E.; Lloyd, D.; Hayes, A.J.; Wainwright, S.D.; Mottram, H.J.; Coles, S.J.; Horton, P.N.; Pope, S.J.A. *Inorg. Chem.* **2015**, *54*, 6606
[38] Elmasides, C.; Kondarides, D.I.; Grunert, W.; Verykios *J. Phys. Chem. B* **1999**, *103*, 5227